Adhesive performance of mushroom-shaped micro-pillars with interfacial micro-bubbles of air

Elena Pierro[1),*], Giuseppe Carbone[2)], Luciano Afferante[2)] and Francesco Bottiglione[2)]

[1)]Università degli Studi della Basilicata, Scuola di Ingegneria, Via dell'Ateneo Lucano 10, Potenza, Italy
[2)]Politecnico di Bari, Dipartimento di Meccanica, Matematica e Management, V.le Japigia 185, Bari, Italy
[*]Corresponding author: elena.pierro@unibas.it

1. Introduction

Microstructured adhesive surfaces, inspired by some biological attachment systems (e.g. Gecko foot pad) often exhibit extremely high adhesive performance [1,2]. Recent experimental observations [3] have shown that mushroom shaped microstructures [Figure 1-(a)] strongly outperform, in terms of adhesive properties, surfaces covered with miniaturized flat-punches [Figure 1-(b)] made of the same material (polyvinylsiloxane (PVS), Young's modulus E = 3MPa).

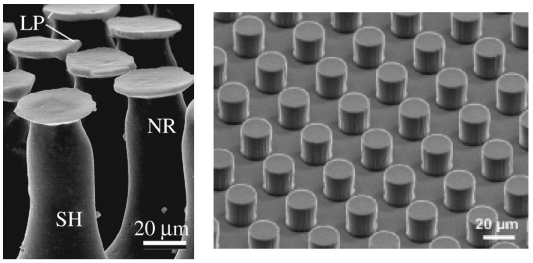

Figure 1: A SEM image of microfabricated PVS mushroom shaped pillars (courtesy of prof. Gorb): LP, contact plate lip; NR, narrow neck; SH, pillar shaft, (a); a SEM image of a microstructured surface with flat punch (adapted from Ref. [3]), (b).

Recently the authors [4] have clarified the physical mechanism providing mushroom shaped micro-pillars with superior adhesive performance compared to cylindrical micro-pillars. In fact these type of micro-pillars present much lower adhesive strength as they usually debond because of crack propagation from the external perimeter (mode I mechanism) [Figure 2].

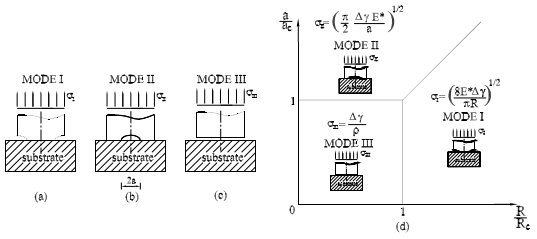

Figure 2: Debonding of a flat punch pillar may occur because of crack propagation from the pillar edge (a), nucleation and propagation of interfacial defects (b), decohesion due to the achievement of the theoretical contact strength (c). Map of debonding mechanisms of a flat punch (d).

Optimal mushroom shapes, on the contrary, usually detach because of the propagation of existing interfacial defects, e.g. dust particles or solid impurities (mode II debonding) [see Figure 3].

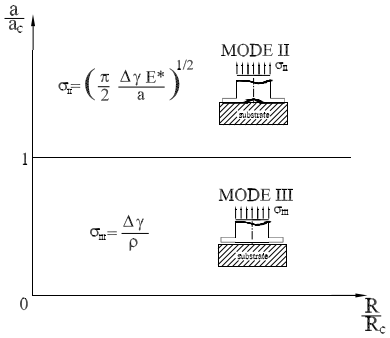

Figure 3: Map of debonding mechanisms for an optimal mushroom shaped pillar. Detachments in this case must be governed by mode II or mode III debonding, depending on which one of them is energetically more favorable.

However, even on perfectly clean surfaces, micro-nano-bubbles of air might form during the initial approach of the micro-pillar to the substrate. These bubbles may strongly reduce the adhesive strength of the system. In this paper, we focus on this aspect of micro-pillar adhesion. With this scope in mind, we first calculate the interfacial energy of the system, then we determine the equilibrium conditions depending on the applied tractive stress and initial size of the entrapped air bubble.

We calculate the critical pull-off stress as a function of the initial volume of the entrapped air, and compare these results with those obtained when, instead of air, small external solid particles are entrapped at the interface. Our results show that the presence of entrapped air is more critical since it strongly reduces the suction effect. The critical stress, indeed, is about 35–40% smaller than the value observed in the case of solid particles.

2. The total interfacial energy of the system

In order to carry out the analysis we need to precisely calculate the total energy change of the system when a bubble of air is present at the interface. We assume that the bubble of air is much smaller than the diameter and

height of the pillar so that one can treat the pillar as an elastic half-space in contact with a rigid flat surface. We assume isothermal conditions and a constant uniform asymptotic far field tractive stress σ, so that the equilibrium of the system can be sought by requiring that the total free energy at the interface (i.e. the interfacial Gibbs energy) is stationary. Given the defect size and assuming a linear elastic material, the calculation of the energy change of the system must consider four different contributions (see also [5] for a different derivation): (i) the contribution to the interfacial elastic energy due to the asymptotic applied uniform tractive stress σ, (ii) the contribution to the interfacial elastic energy due the air pressure p, (iii) the internal energy of the air bubble, (iv) the variation of surface energies due to the presence of van der Waals forces. Let us consider the system shown in Figure 4, where the bottom (initially flat) surface of an elastic half-space is glued to a rigid plate except on a circular region of radius a. Let us displace the rigid plate of a quantity u_0 (see Figure 4) so that a small void is formed at the interface. Assume that the air pressure in the void is p.

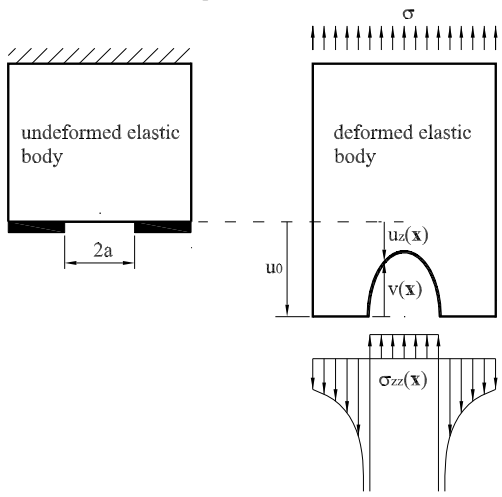

Figure 4: The displacement, gap and stress distributions involved in the calculation of the free interfacial energy.

To calculate the elastic energy of the system, let us first observe that the contact problem may have an equivalent formulation in terms of interfacial elastic energy, i.e. in terms of the amount of elastic energy stored at the interface as a consequence of local interfacial deformations [6]. Accordingly, the elastic interfacial energy is [6].

$$U_{el} = \frac{1}{2}\int d^2x \sigma_{zz}(\mathbf{x})\left[u_z(\mathbf{x}) - \langle u_z(\mathbf{x})\rangle\right] \tag{1}$$

where $\mathbf{x}$ is the in-plane position vector, $\sigma_{zz}(\mathbf{x})$ is the non uniform normal interfacial stress, $u_z(\mathbf{x})$ is the local normal displacement of the surface, and $\langle u(\mathbf{x})\rangle$ is the average displacement at the interface (the symbol $\langle\cdot\rangle$ is the average operator). Considering that because of force balance the uniform stress σ at infinity is $\sigma = \langle\sigma_{zz}(\mathbf{x})\rangle$ one can rephrase Eq. 1 as

$$U_{el} = \frac{1}{2}\int d^2x \left[\sigma_{zz}(\mathbf{x}) - \sigma\right]u_z(\mathbf{x}) \tag{2}$$

Now let us define (see Figure 4) the gap distribution $v(\mathbf{x})$ as $v(\mathbf{x}) = u_0 - u_z(\mathbf{x})$. Of course $v(\mathbf{x}) \neq 0$ on the circular region of radius a, whereas it vanishes elsewhere. Using $v(\mathbf{x})$ and considering that $\sigma_{zz}(\mathbf{x}) = -p$ for $|\mathbf{x}| < a$, Eq. 2 becomes

$$U_{el} = \frac{1}{2}(p+\sigma)V \tag{3}$$

where $V = \int d^2x v(\mathbf{x})$ is the volume of the air bubble. The total Helmholtz free interfacial energy F is then the sum of the elastic interfacial energy, the free internal energy $U_A = -p_0 V_0 \ln(V/V_0)$ of the entrapped air, and the surface energy, i.e.

$$F(V,a) = U_{el}(V,a) + U_A(V) + \pi a^2 \Delta\gamma \tag{4}$$

From thermodynamics one concludes that under isothermal conditions and constant bubble volume V the equilibrium of the system corresponds to the stationary values of the energy F. However, in our analysis we keep constant the asymptotic load $\langle\sigma(\mathbf{x})\rangle = \sigma$. In this case the equilibrium of the system corresponds to the stationary values of the interfacial Gibbs energy $G(\sigma,a)$. Following the standard approach of thermodynamics [7], we obtain $G(\sigma,a)$ by enforcing a Legendre transformation, i.e.

$$G(\sigma,a) = F(V,a) - \left.\frac{\partial F}{\partial V}\right|_a V \tag{5}$$

Observing that $\partial U_{el}/\partial V|_a = p + \sigma$ and $\partial U_A/\partial V|_a = -p$, one yields the required expression for the interfacial Gibbs energy G, i.e.

$$G(\sigma,a) = \Delta U_{tot} = \frac{1}{2}(p-\sigma)V + U_A + \pi a^2 \Delta\gamma \tag{6}$$

Beside Eq. 6 two additional equations are needed

$$pV = p_0 V_0 \tag{7}$$

and

$$V = \frac{8a^3}{3E^*}(\sigma + p) \tag{8}$$

where $E^* = E/(1-\mu^2)$, μ is Poisson's ratio. Eqs. 7,8 allow to calculate the quantity V and p as a function of the radius a of the non contact circular area. Therefore, the total energy change ΔU_{tot} given by Eq. 6 finally depends only on the applied constant stress σ and the size of the voids a. By following a similar approach as in JKR theory [8], requiring that $\partial\Delta U_{tot}/\partial a|_\sigma = 0$ allows to calculate the values of a at equilibrium, given the applied uniform stress σ. The

critical pull-off stress σ_{cr}, which destabilize the defect and causes the detachment of the pillar from the rigid flat substrate, is determined by requiring that at equilibrium the relation $\partial^2 \Delta U_{tot} / \partial a^2 \big|_{\sigma} = 0$ is also satisfied.

The above equations can be rephrased in a dimensionless form. To this end let us define the adhesion length $\delta = \Delta\gamma / E^*$ and the dimensionless quantities $\tilde{\sigma} = \sigma / E^*$, $\tilde{p} = p / E^*$, $\tilde{a} = a / \delta$, $\tilde{V} = V / \delta^3$. The dimensionless total energy change of the system is therefore $\Delta \tilde{U}_{tot} = \Delta U_{tot} / \left(\delta^3 E^*\right)$, where $\tilde{V} = (8/3)(\tilde{\sigma} + \tilde{p})\tilde{a}^3$ and $\tilde{p}\tilde{V} = \tilde{p}_0 \tilde{V}_0$.

3. The critical stress

In order to calculate the critical stress and the critical air bubble size, we assume that the environment pressure is $1bar$, so that the initial pressure of the entrapped air bubble is also $p_0 = 0.1MPa$. We also notice that the asymptotic applied stress σ is $\sigma = \sigma_0 - p_0$, where $\sigma_0 = P / A$ is the external applied average stress, P the applied load and A the cross section area of the pillar. Figure 5 shows the total dimensionless energy change $\Delta \tilde{U}_{tot}$ as a function of the dimensionless radius $\tilde{a}$, for different values of the initial dimensionless size $\tilde{a}_0$ of the void. In our calculations we have used $\sigma = 0.2MPa$ (i.e. $\sigma_0 = 0.3MPa$), $\Delta\gamma \approx 16mJ / m^2$, $E = 3MPa$ and $\nu = 0.5$.

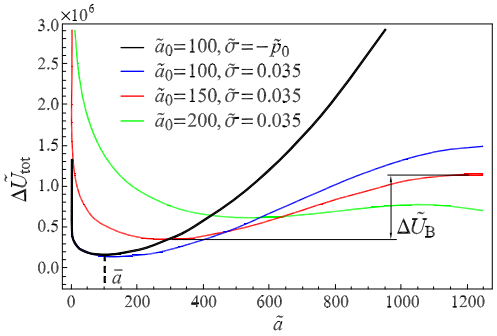

Figure 5: The dimensionless total energy $\Delta \tilde{U}_{tot}$ as a function of the radius of the detached area $\tilde{a}$, for three different values of the initial radius $\tilde{a}_0$, given the same value of dimensionless stress $\tilde{\sigma} = 0.035$ (blue, red and green curves). Increasing $\tilde{a}_0$ determines a decrease of the energy barrier $\Delta \tilde{U}_B$ between the stable and unstable equilibrium states. The solid black curve represents the total energy as a function of $\tilde{a}$ when the pillar is subjected to the environment pressure only, i.e. $\tilde{\sigma} = -\tilde{p}_0$, and for $\tilde{a}_0 = 100$. Notice that in this case there is only one equilibrium condition at $\tilde{a} = \bar{a}$ which is necessarily stable.

The figure shows that for any value of $\tilde{a}_0$, two equilibrium conditions exist, i.e. the stable state (energy minimum) and the unstable state (energy maximum). However, as expected, when the asymptotic applied stress is zero or even negative only a stable equilibrium state must be present (see the black line in Figure 5 with $\tilde{a}_0 = 100$ and $\tilde{\sigma} = -\tilde{p}_0$, i.e. $\tilde{\sigma}_0 = 0$). When an external stress $\sigma > 0$ is applied, an energy barrier must be exceeded in order to destabilize the system. The energy barrier $\Delta \tilde{U}_B$ in this case is defined as the difference between the energy value of the unstable equilibrium state and the energy value of the stable equilibrium state. From Figure 5, given the same applied stress, one observes that the energy barrier $\Delta \tilde{U}_B$ decreases as the initial radius $\tilde{a}_0$ of the bubble (i.e. its initial volume) is increased. When $\Delta \tilde{U}_B = 0$, i.e. when $\partial \Delta U_{tot} / \partial a \big|_{\sigma} = 0$ and $\partial^2 \Delta U_{tot} / \partial a^2 \big|_{\sigma} = 0$, the critical defect size $(\tilde{a}_0)_{cr}$ is found which prevents the pillar from adhering to the substrate.

Given the initial defect size $\tilde{a}_0$, it is also interesting to analyze what happens when the applied stress σ is increased. In particular, Figure 6 shows that, for a fixed value of the radius $\tilde{a}_0$ (we have considered $a_0 = 0.6\mu m$, i.e. $\tilde{a}_0 = 150$), when the applied stress σ increases an unstable equilibrium state appears, which is again separated from the corresponding stable equilibrium by an energy barrier $\Delta \tilde{U}_B$. As the stress $\tilde{\sigma}$ is further increased, the energy barrier $\Delta \tilde{U}_B$ decreases and vanishes at a certain stress level $\tilde{\sigma}_{cr}$ (the so called critical pull-off stress) at which the air bubble of initial size $\tilde{a}_0$ is destabilized and the pillar detaches from the substrate.

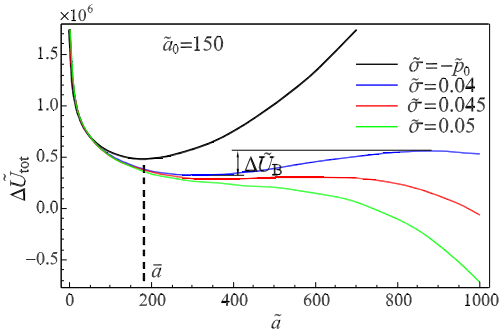

Figure 6: The dimensionless total energy $\Delta \tilde{U}_{tot}$ as a function of the radius of the detached area $\tilde{a}$, for four different values of the applied stress $\tilde{\sigma}$, and for $\tilde{a}_0 = 150$. Increasing $\tilde{\sigma}$ determines a decrease of the energy barrier $\Delta \tilde{U}_B$ between the stable and unstable equilibrium states until it vanishes and the air bubble is destabilized.

4. Comparison with solid defects

We now compare the critical stress in case of solid defects of size a_S (dust particles, impurities, etc.) $\sigma_{II} = \left[\pi \Delta\gamma E^* / (2a_S)\right]^{1/2}$ with the critical pull-off stress σ_{cr} obtained in the case a bubble of air entrapped at the interface. The comparison must be carried out assuming that, at $\tilde{\sigma} = -\tilde{p}_0$ (i.e. $\tilde{\sigma}_0 = 0$), the (dimensionless) size $\bar{a}$ of the air bubble at equilibrium is identical to the (dimensionless) solid defect size, i.e. $\bar{a} = \tilde{a}_S$. Figure 7 compares the critical stress $\tilde{\sigma}_{0cr} = \tilde{\sigma}_{cr} + \tilde{p}_0$ in the two cases as a function of the radius $\bar{a}$.

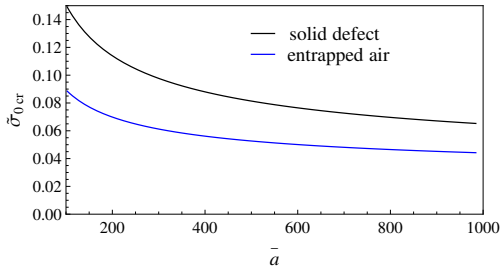

Figure 7: The dimensionless external critical stress $\tilde{\sigma}_{0cr} = \tilde{\sigma}_{cr} + \tilde{p}_0$ as a function of the air bubble or solid particle size $\bar{a}$. The blue curve refer to the air bubble case, the black curve to the interfacial solid particle case.

We observe that, in the case of air bubble, the debonding stress $\tilde{\sigma}_{0cr}$ is always significantly smaller than the one obtained in the case of solid defects with a reduction of about 35-40% over the entire range of defect size considered in the calculation, i.e. $\bar{a} = \tilde{a}_S = 0.4 - 4\mu m$. Indeed, micro-air bubbles weaken the adhesive link between the pillar and the rigid substrate more than the presence of external particles, since their gas pressure exerts an additional debonding force and reduce the suction effect which contributes to keep the pillar in contact with the substrate. This represents a practical problem during fast attaching-detaching of this kind of microstructure, since in this case the entrapment of air can hardly be avoided.

5. Conclusions

In this paper, we study the influence of interfacial micro-bubbles of air on the adhesive perfomance of micro- mushroom-shaped pillars. We show that, in absence of an applied load, the micro-bubble remains in stable equilibrium. However as soon as an external tractive stress is applied to the pillar, an unstable equilibrium condition appears. It follows that a critical pull-off stress exists which destabilize the air bubble and causes the complete detachment of the pillar from the substrate. We calculate this critical pull-off stress and we show how it depends on the initial volume of entrapped air. Of course, increasing the amount of entrapped air leads to a significant reduction of the pull-off stress. Interestingly our results have highlighted that the air bubbles at the interface are more critical than the presence of interfacial solid defects of same size. This means that to achieve the highest adhesive performance the approach of the pillar to the substrate must be carried out very carefully, to avoid entrapment of air at the interface.

6. References

[1] C. Majidi, R. E. Groff, Y. Maeno, B. Schubert, S. Baek, B. Bush, R. Maboudian, N. Gravish, M. Wilkinson, K. Autumn, R. S. Fearing, Phys. Rev. Lett., 2006, 97, 076103.

[2] A.K. Geim, et al., Nature Materials, 2003, 2(7), 461.

[3] C. Greiner, A. del Campo, E. Arzt, Langmuir, 2007, 23, 3495-3502.

[4] G. Carbone, E. Pierro, N. Gorb, Soft Matter, 7, 5545-5552 (2011).

[5] G. Carbone, E. Pierro, Soft Matter 8, 7904–7908 (2012).

[6] G. Carbone, L. Mangialardi, J Mech Phys Solids 56(2), 684–706 (2008).

[7] Callen HB (1985) "Thermodynamics and an introduction to thermostatistics" Wiley, USA ISBN 0-471-86256-8.

[8] Johnson KL, Kendall K, Roberts AD (1971) Proc R Soc Lond A 324:301–313.